Research article

Non-destructive characterization of physical and chemical clogging in cylindrical drip emitters

Venkata Ramamohan Ramachandrula [a,b,*], Ramamohan Reddy Kasa [c]

[a] Water and Livelihoods Foundation (WLF), 12-13-451, Street no.1, Tarnaka, Secunderabad, 500017, India
[b] Research Scholar, JNTU, Hyderabad, 500085, India
[c] Centre for Water Resources (CWR), Institute of Science and Technology (IST), JNTU, Hyderabad, 500085, India

ABSTRACT

Characteristics and deposition pattern of clogging material on cylindrical drip emitters was studied using non-destructive methods of evaluation. Two sets of four cylindrical emitter samples were collected from farm lands. One set of sample emitters was analyzed using Computed Tomography (CT). Other set was dissected and the clogging material extracted was analyzed using Energy Dispersive X-Ray Fluorescence (EDXRF) and X-Ray Diffraction (XRD). CT scans revealed the geometric properties of emitters and the spread of clogging material on the emitter surface. EDXRF analysis found statistically significant inverse relationship between the proportion of physical clogging and chemical clogging materials. XRD analysis indicated presence of physical and chemical clogging materials in their crystalline forms. Emitters having transverse flow path and the boundary optimized with curvature found with the least deposition of physical clogging materials. Corresponding proportion of chemical clogging (as Ca) was found to be much higher. All the samples were found with more clogging material closer to the outlets. Efforts to optimize emitter geometry shall also take into account the outlet area optimization and chemical clogging for obtaining best results.

1. Introduction

Drip irrigation systems are efficient in application of irrigation water to crops and are widely adopted all over the world. A gauge pressure of 100–150 kPa (10–15 m of pressure head) is maintained in the drip system to deliver water uniformly across the agriculture land. Groundwater is the major source of water for drip systems in India. Emitter is an important component in the drip irrigation systems to deliver water to plants after necessary dissipation of pressure. The emitter surface is typically provided with labyrinth flow paths for dissipation of pressure while water passes through it. Clogging of drip emitters is a major problem that affects the emitter discharge, uniform delivery of irrigation water over the farm land and ultimately its functional life.

Emitter clogging and its impacts on the water discharge from drip systems has been studied extensively by various researchers. Bucks et al. (1979) classified the emitter clogging into physical, chemical and biological forms, whose relative intensities vary for different source water qualities. In case of groundwater sources, physical and chemical clogging assumes dominance, while biological clogging plays significant role in case of recycled waste water. The intensity of clogging is not uniform across the lateral pipes in a given drip irrigation system. While studying clogging of drip emitters used in sugar cane cultivation, Bui (1988) observed that clogging is more severe in emitters at the end of lateral lines than at the beginning. Carbonates of Calcium (Ca) and Magnesium (Mg) are the predominant sources of chemical clogging. Higher temperature and pH reduce Calcium Carbonate ($CaCO_3$) solubility in water, hence are favorable conditions for $CaCO_3$ to precipitate (Nakayama and Bucks, 1991). Liu and Huang (2019) experimentally found that the higher pH and dissolved salts in the source water have causal effect on chemical clogging of emitters. Kirnak et al. (2004) determined emitter uniformity coefficient and exponent values at varying pressure conditions using small-scale laboratory experiments. Wei et al. (2008) used both simulations and lab experiments to study clogging behaviour of emitters. Yavuz et al. (2010) tested emitters collected from farm fields to determine the decline in uniformity coefficient over years of use. de Camargo et al. (2014), Bounoua et al. (2016) and Krishna Reddy et al. (2017) studied the impairment of emitter discharge due to different forms of emitter clogging by measuring discharge and uniformity of delivery. Shaw et al. (2018) determined the improvement in emitter discharge after chlorination in laboratory settings. Feng et al. (2019)

attempted to quantify the randomness in composite clogging behaviour of different types of emitters. Ramachandrula and Kasa (2019a) carried out an exploratory study on causes of chemical clogging and patterns of deposition on emitter sections.

Another area of past work is the study of two-phase flows - flow of physical impurities with water - in emitters. Few researchers conducted clogging tests on strip-type emitters with input water mixed with physical impurities followed by Computational Fluid Dynamics (CFD) modelling. Li et al. (2008), Feng et al. (2013), and Yu et al. (2018), using CFD and Particle Tracking Velocimetry (PVT) techniques, analyzed emitter clogging mechanisms when physical particles of different sizes were introduced into water. Li et al. (2006), Dazhuang et al. (2007), Reethi et al. (2015) and Yang et al. (2020) studied the anti-clogging performance of flat emitters with different dent features, such as, angles, spacing, height and depth of flow passage. Patil et al. (2013) carried out laboratory hydraulic and clogging studies and compared them with CFD models of emitter flow characteristics. Findings of Feng et al. (2018) and Li et al. (2019a) on desirable geometric properties for anti-clogging emitters are specifically relevant to the current study. Feng et al. (2018) dealt with CFD analysis and design of efficient and self-cleaning emitter dentate paths for flat emitters. They compared 'main channel' and 'washing the wall with vortex' design methods and concluded that boundary optimization using small arcs betters anti-clogging performance. Li et al. (2019a) conducted short-duration experiments, with different source waters, on different flat emitter models and concluded that anti-clogging performance of emitters improved with increasing average cross-sectional flow velocity in labyrinth paths.

Since the in-line emitters are enclosed by the Poly Ethylene (PE) lateral tubes, the emitter surface is not visible to naked eye. It is difficult to physically dissect the lateral tube without disturbing the deposits on emitter surface. Non-Destructive Testing and Evaluation (NDTE) is a very useful branch of science whose applications are well-known in studying of composite materials; understanding material compositions and in fault analysis. Recent studies demonstrate applications of NDTE in soil drainage properties and water flow through porous media (Nguyen and Indraratna, 2019). Applications of NDTE to understand drip emitter clogging patterns was explored by only few researchers. Liu et al. (2015) and Liu et al. (2018) analyzed the chemical clogging patterns of drip emitters in laboratory settings by physical dissection followed by Field Emission Scanning Electron Microscope (FESEM). Li et al. (2019b) analyzed the chemical composition of emitter clogging material using XRD at different degrees of clogging. This study did not relate the geometry of emitter and degree of clogging. However, Zhangzhong et al. (2019) established that both level of dissolved salts and the emitter type influence the kinetics of chemical clogging while using saline water.

Computed Tomography (CT) is a non-destructive technique for visualizing interiors of solid composites with distinct X-ray attenuation properties. CT has been widely applied in material testing, identification of faults in industrial products, examination of geological materials etc. Ramachandrula and Kasa (2019b) scanned clogged emitters using a CT scanner and studied the spread of emitter clogging material with reference to the geometry of emitter flow paths. Xiao et al. (2020) used the CT technique to visualize the spatial distribution of biofilms on drip emitters and suggested optimum emitter flow channel structures. Zhou et al. (2018) carried out laboratory studies on drip systems using reclaimed water and identified mineral constituents of emitter clogging substances using NDTE methods, such as, XRD. However, sparse availability of CT scanners and prohibitive costs of scanning are impediments to studies that necessitates NDTE analysis of several samples.

Current study has the objective of exploring the relationship between the emitter geometry and clogging patterns on the emitter surface using NDTE techniques. The study picked up emitters used for several years by farmers under field conditions, in contrast to the short-cycle laboratory studies. While most of the earlier studies focused on flat in-line emitters, current study deals with cylindrical inline emitters that are most widely used in India. Current study blends the field-oriented study with CT scanning of emitters, followed by extraction of clogging material for analysis using EDXRF and XRD techniques. While most of the emitter clogging studies confined to study of physical clogging on labyrinth paths, current study includes outlet areas and chemical clogging as well.

2. Materials and methods

2.1. Field study and sampling

A contiguous cluster of five villages in Gundala *mandal*[1], Yadadri Bhongir district, Telangana State, India was taken as study area. The area of the cluster is approximately 7 km^2, rectangular area bounded between 17.55327°N, 79.15593°E and 17.55605°N, 79.19385°E. The study area is predominantly of hard-rock geology with fractured granitic aquifers facilitating groundwater availability and movement. Soils in the study area are of red sandy loam type with good drainage and infiltration properties. Average annual rainfall in the area is about 750 mm, mostly during June–September period. Paddy, Cotton, Maize, Vegetables and Mango are the major crops grown in these villages. There are around 70 farms where drip irrigation systems were installed by farmers in the study area. During the field study done in April 2019, four drip systems among them were chosen based on their continuous use over years and the incidence of clogging reported by the farmers (Table 1). These drip systems were in use for two to five years as on the date of field study.

All these sample drip systems have lateral tubes with in-line emitters at 1.00 m spacing. Lateral tubes and emitters are made of Linear Low-Density Poly Ethelene (LLDPE) material. All the sample drip systems have non-pressure-compensating emitter with a nominal discharge of 4.00 L h^{-1}. All the drip systems have screen filters of opening size 100 μm for filtering suspended solids (SS) in the source water. Sample drip no.1 has additional sand filters for effective screening of SS from the source open well (OW). Farmers of these four systems never carried out any chemical treatments for removing CaCO$_3$ or SS clogging during the usage of drip systems. However, they all used to flush out the lateral tubes by opening end-caps 3–4 times in a year.

Emitter with outer lateral tube is referred as 'emitter assembly' and the inner emitter alone is referred as 'emitter' henceforth for making the distinction between them. Figure 1(a) depicts various surface features of typical cylindrical emitters. Both the emitters in Figure 1(a) show emitter flow paths in longitudinal direction (i.e., along the flow in the lateral tube). This is true for sample emitters 1,3 and 4. But the sample emitter 2 has flow paths in transverse direction. Emitter 1 has triangular-shaped right-angled dents, but sample emitters 2, 3 and 4 have triangular-shaped ones.

For each of the four sample drip systems, two emitter assemblies were randomly cut from the lateral tubes and preserved for analysis in the laboratory. Figure 1(b) shows one of the emitter samples having an outlet on one side and one of the emitter samples having outlets on both sides. For each visible outlet in Figure 1(b), there is one more, for all the sample emitters, on the other side of cylindrical surface. Out of the total eight sample emitter assemblies, one set of four was used for CT scanning and another set was used for extracting the clogging material and examination using EDXRF and XRD. Thus, the sampling of emitters was randomized spatially and temporally from a compact geographical area.

2.2. Water quality analysis of source water

Groundwater samples from all four source wells of sample drip systems, one per each source, were collected after the water passed through the sand and screen filters during April 2019. These water samples were tested for pH and Total Dissolved Solids (TDS) using Hanna HI98130 field tester at the farm sites. At the laboratory, Total Hardness (TH) was measured by EDTA titration method using Hanna test kit HI3812 and

---

[1] *Mandal* is a geographical unit at the sub-district level.

Table 1. Details of sample drip irrigation systems.

Drip sample no.	Source of water[a]	Year of installation	Make[b]	Years of use
1	OW	2014	Jain	4
2	BW	2013	Jain	5
3	BW	2017	Godavari	2
4	BW	2016	Godavari	3

[a] OW stands for shallow open well with maximum depth of 15 m. BW stands for bore well that are drilled into the hard-rock aquifers up to a depth of 150 m.
[b] The short name of each drip manufacturing company. All drip systems were manufactured in India.

cross-checked with the test kit HI3841. Phenolphthalein Alkalinity (PA) and Total Alkalinity (TA) were measured using Hanna test kit HI3811. SS was measured using the gravimetric method as per the Method 2540D of APHA (2012). Stoichiometric classification of TA into three principal forms - Bicarbonate, Carbonate and Hydroxide - were done using Alkalinity relationships suggested by Method 2320 of APHA (2012). Further, Carbonate Hardness (CH) and Non-Carbonate Hardness (NCH) were derived using known relationship between TH, Bicarbonate Alkalinity (BA) and Carbonate Alkalinity (CA).

2.3. Characterization of clogging material deposition patterns

Four emitter assemblies were scanned using Computed Tomography (CT) Mini equipment, Procon GmbH make, with X-ray energy set at 121 kV and current at 119 μA. The equipment consisted of a micro focus X-ray tube (7-micron focal spot) and a Hamamatsu flat panel detector (1024 × 1024 photo-diodes). The equipment has a maximum resolution of 14 μm. The X-ray beam penetrates the sample and assigns an intensity value on grayscale for each volume element (voxel) based on its X-ray attenuation property, which is closely related to its density and composition. The intensity values for each voxel were stored in a series of two-dimensional (2D) sections in X-Y, Y-Z and X-Z planes. Finally, these 2D sections were assembled as a single three-dimensional (3D) image of the emitter assembly. The 3D images of the emitter assemblies were further processed using Dragonfly Software ver. 4.1.0.647, by Object Research Systems (ORS) Inc., Canada. While the material density of the outer lateral tube and inner emitter were found to be in close range, the density of the clogging material was much higher compared to them. Due to the lack of attenuation contrast, the outer layer could not be separated from the emitter using the partitioning of intensity ranges.
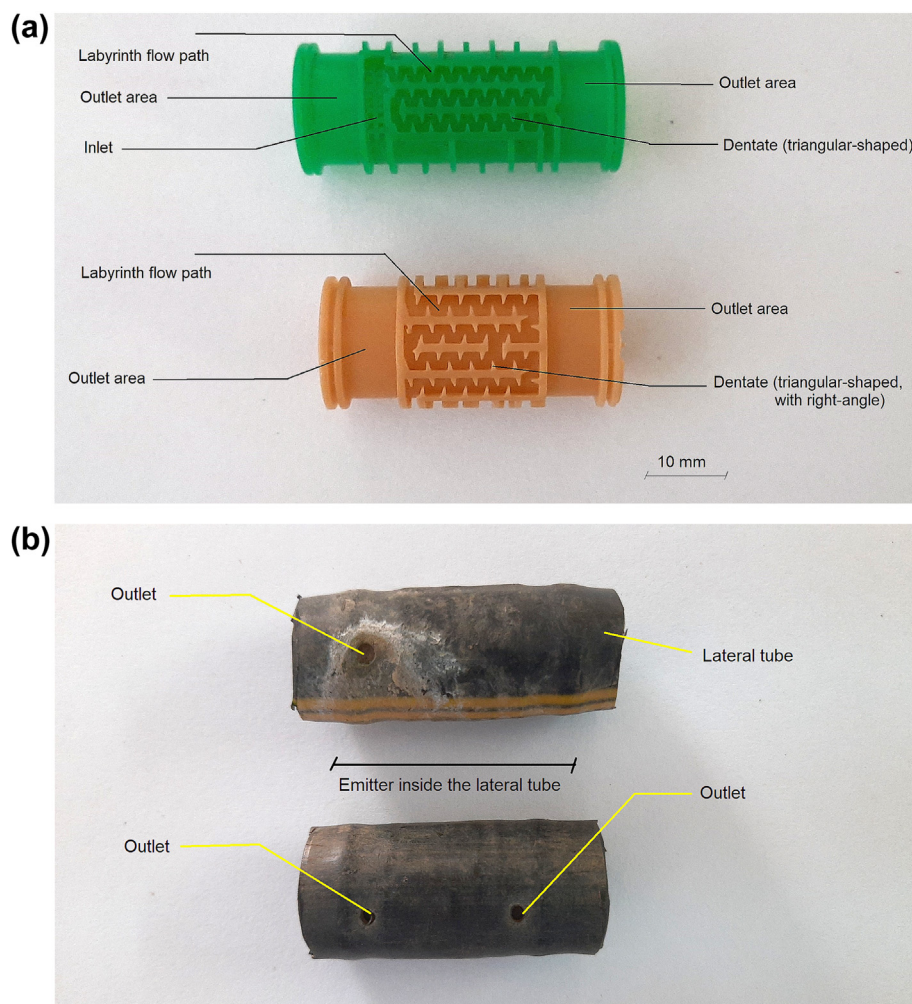
Figure 1. Surface features of (a) cylindrical emitters and (b) emitter assembly.

The raw data in grayscale format were rendered with 'hot metal' color scheme; applied 'windows levelling' for improving the contrast; and applied 'slicing tools' in order to slice the cylindrical emitter into two half-cylinders. Sliced views of labyrinth flow paths were generated as well as inlet and outlet areas were marked. The clogging material in the flow paths as well as closer to the inlet and outlet areas was distinctly colored and identified. Some of the clogging material deposited on the inner surface of the emitter, which is in direct contact with the water flowing in the lateral tube, was also identified. Finally, two pictures of each emitter, representing emitter flow paths on either side of the cylindrical surface, were extracted. These two pictures of each emitter are designated as side 1 and side 2. All these figures were rendered to a common scale to facilitate comparison. The flow path width (b), dentate height (h), dentate angle (Θ) and dentate spacing (s) were measured using 2D sectional images (Figure 2).

2.4. Chemical composition of clogging material

The outer lateral tube of four emitter assemblies was cut open and the clogging material in powder form was manually extracted. Depending on the amount of deposited material found on the emitter, the quantity of extracted material also varied. However, entire amount of clogging material could not be accessed and extracted from the emitter surface, as the emitter was firmly fixed inside the lateral tube through an extrusion process at the time of manufacture.

Visual observation revealed that the extracted powders are light brown in color, with the presence of white-colored particles and flakes. The powders contained a mix of fine silt and clay particles, which passed through the screen filters of 100 μm size fitted to the drip system as well as the fraction of chemical precipitate from water. Figure 3(a), (b), (c), (d) display the dissected emitter assemblies and the powder samples extracted from them. In addition, the white precipitate near the outlets of all four emitter assemblies was extracted and mixed as sample 5 (Figure 3(e)). This is presumed to be $CaCO_3$ formed as a result of exposure to sunlight and evaporation of water droplets that remained on the emitter tube.

All five clogging material samples were first analyzed for their elemental composition using desktop EDXRF equipment, model EDX-8000 of Shimadzu make. Incident X-rays were produced using Rh target at 15 kV for elements C–Sc and at 50kV for elements Al–U. The emitted radiation was measured in the energy range of 0–40 keV. The presence of 17 different elements, as mass percentage, was obtained for each of the five samples. Ignoring the trace constituents with <1.00% magnitude, linear correlation between five major elements - Silicon (Si), Aluminum (Al), Potassium (K), Iron (Fe), Calcium (Ca) - was studied. Corresponding p-values for each correlation coefficient was calculated using two-tailed Student t-distribution.

Taking clue from the elemental composition detected from EDXRF analysis, the powder samples were analyzed for crystalline properties of different unknown components. Powder XRD, model D-8 Advance A25 with an advanced Lynx-Eye Detector, of Bruker make was used for this analysis. Experimental settings were - X-ray beam energy 40 kV; current 30 mA; monochromatic wavelength of X-rays at 1.5406 Å and 2Θ ranging between 2° to 80° with a step size of 0.02°. Bragg's Law, which relates the wavelength of X-ray radiation to the diffraction angle and the lattice spacing in the crystal sample, forms the basis for this analysis (Bunaciu

et al., 2015). Qualitative phase analysis was performed using TOPAS software that came with the XRD equipment, using the International Centre for Diffraction Database (ICDD) PDF-4 database. Dominant phases of major crystalline components were identified for each powder sample using the Rietveld refinement method. Apart from crystalline phases of different chemical compounds, there is a possibility of presence of amorphous components also in the sample. Quantification of phases may be erroneous due to the normalization performed in the quantitative refinement process. Therefore, no attempt was made to quantify the crystal phases.

3. Results

3.1. Groundwater quality analysis

Table 2 presents the water quality test results of samples collected from four source wells. Sample 1 is from a shallow OW and three others are from deep bore wells (BWs). The pH values of the groundwater samples ranged from 7.28 to 7.64, which is quite normal. SS value of water from the OW is higher than that of water from BWs. Within BWs, SS varied in a narrow range of 10.0–11.6 mg L^{-1}. The measured TDS values varied widely from 860 to 1230 mg L^{-1}. The TDS and TH of water sample from the OW is quite higher compared to the other BW sources. Repeat sampling and testing confirmed this result. Such a high TDS in an OW is an abnormality and contradicts the general notion that OWs will have lower TDS and TH values compared to BWs.

Three of the water samples, 2,3 and 4, have CH more than 400 mg L^{-1} while sample 1 has the lowest CH of 280 mg L^{-1}. Except for the sample 1, the NCH has no significant presence in the water samples. Since pH and CH are known as causative factors in chemical clogging of emitters, later sections examined the relation between the amount of Ca found in the clogging material of different emitters with the variation of pH and CH in the irrigation water samples.

3.2. Geometry and clogging pattern of emitters

Figures 4, 5, 6, and 7 illustrate the emitter surface features as well as the deposition pattern of clogging materials on their surface. Each of these figures presents two views – side 1 and side 2 – of the labyrinth flow paths on either side of the cylindrical emitter. All these views are at a magnified scale as shown on the bottom-left of the figures. The orientation of these views in 3D are represented by an axes-cube at the bottom-right on these figures. The density of the emitters themselves and the clogging material map to an intensity scale, which presents the emitters as lower density material (in shades of black-to-gray) and the clogging material as a relatively dense material (in shades of red-to-yellow). The clogging material identified in these figures is a mixture of physical and chemical clogging materials. The clogging material also varies in density at different parts of the emitters. There is the presence of low-density clogging material in light black/gray color as well as relatively higher density material represented in light to a darker brown color. EDXRF analysis of the clogging materials, discussed in later sections, exposed the chemical composition of this mixture. A significant part of the deposits observed in emitter sample 4 (Figure 7(a)) are, in fact, found not on the emitter flow paths but on the inner cylindrical surface.

Samples 3 and 4 are identical in their geometric properties. But, samples 1 and 2 are different from them. Comparing the geometries of all four emitter samples, they primarily differ in terms of (i) location and number of inlets, (ii) number of outlets, (iii) the orientation of labyrinth flow paths (longitudinal or transverse in relation to the flow direction in the lateral tube), (iv) shape, length and dimensions of the flow path and (v) dentate shape. A concise comparison of these major features as well as the measured dimensions are presented in Table 3.

Compared to 1,3 and 4, emitter 2 stands out in terms of the orientation and width of flow path and curved boundaries. Both the dentate angle and dentate spacing in emitter 2 are much higher compared to the
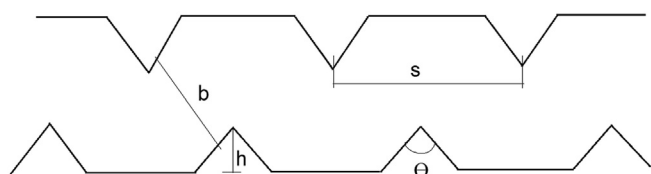
Figure 2. Geometric features of a typical labyrinth flow path.
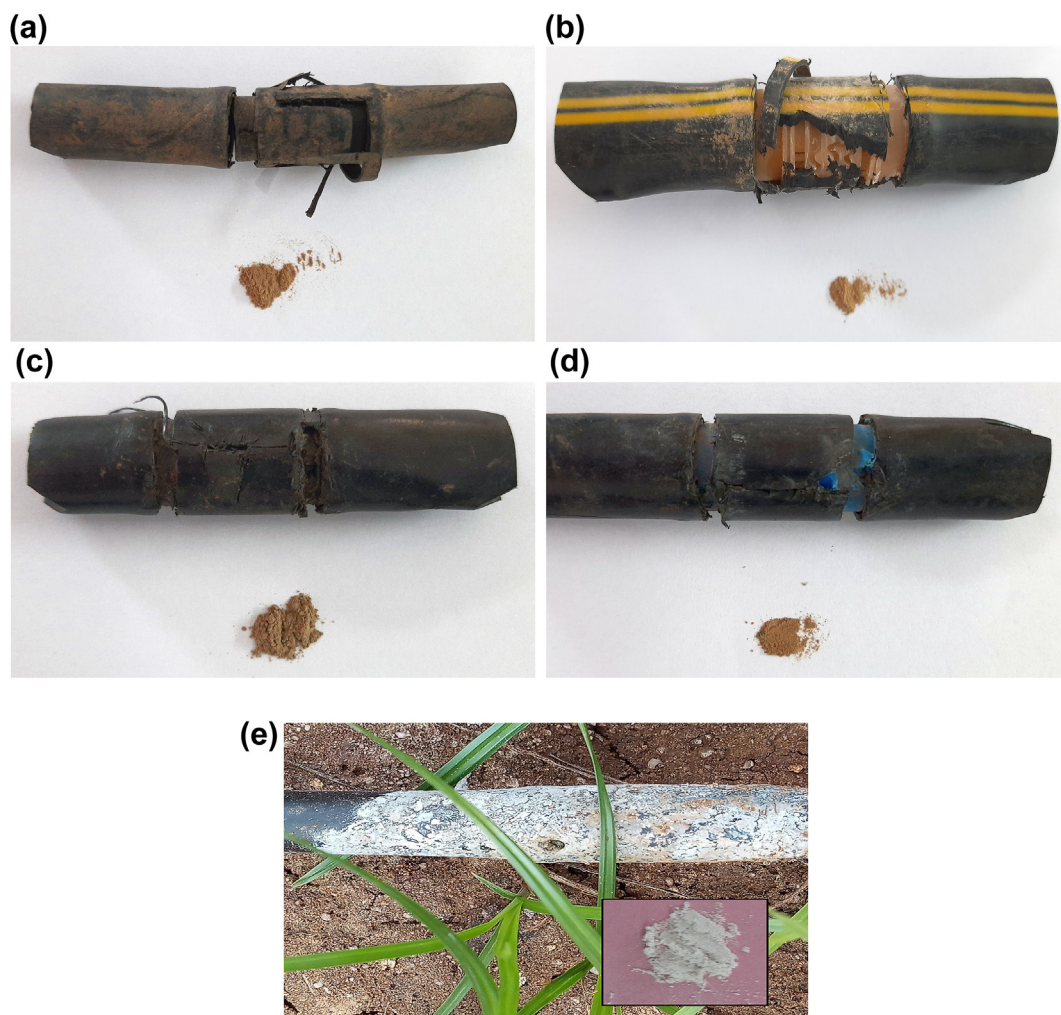
Figure 3. Dissected emitter and extracted clogging material of (a) sample 1, (b) sample 2, (c) sample 3, (d) sample 4 and (e) Sample 5.

other three sample emitters. The quantity of clogging material varied across emitters possibly due to different years of use and differences in anti-clogging performance of different geometries. Visual observation reveals that most of the clogging is towards and on the outlet areas. This indicates that the emitter design optimization needs to ensure that the clogging material is not only flushed out of labyrinth paths but the outlet areas too.

3.3. EDXRF analysis and elemental correlations

Quantity of powder samples extracted from four emitters is not exactly the total quantity of deposits on the emitters. This is due to difficulty in cutting the assemblies and accessing the different parts of the emitters. Therefore, the composition analysis of powder extracts was done on mass percentage basis, instead of attempting absolute

quantification of different constituents of the clogging material. The EDXRF analysis of elemental composition (as mass percentage) in the five powder samples is presented in Table 4.

Out of the 17 elements found in the powder samples, Si, Al, K, Fe and Ca are the five major elements and the rest are trace constituents. For correlation analysis, these five major elements are considered. The linear correlation coefficients and corresponding p-values for the correlation between different pairs of five elements is presented in Table 5. Smaller p-values indicate that the correlation between different elemental compositions is statistically significant. First three elements, Si, Al and K, have fairly significant positive correlation. Fe is found to have significant positive correlation with Si, Al but not with K. Ca has a significant negative correlation with all the other four elements. This indicates that the Ca is not present in any chemical compound in the powder samples, which also has any of the other four elements. It may be inferred that the

Table 2. Water quality test results.

Water Sample no.	pH	SS (mg L^{-1})	TDS (mg L^{-1})	TH (mg L^{-1})	PA (mg L^{-1})	TA (mg L^{-1})	CH (mg L^{-1})	NCH (mg L^{-1})
1	7.30	13.1	1,230	660	0	280	280	380
2	7.64	10.0	910	470	0	408	408	62
3	7.56	11.6	860	420	0	450	420	0
4	7.28	10.2	960	430	0	461	430	0

Note: SS = suspended solids; TDS = total dissolved solids; TH = total hardness; PA = phenolphthalein alkalinity; TA = total alkalinity; CH = carbonate hardness; NCH = non-carbonate hardness.
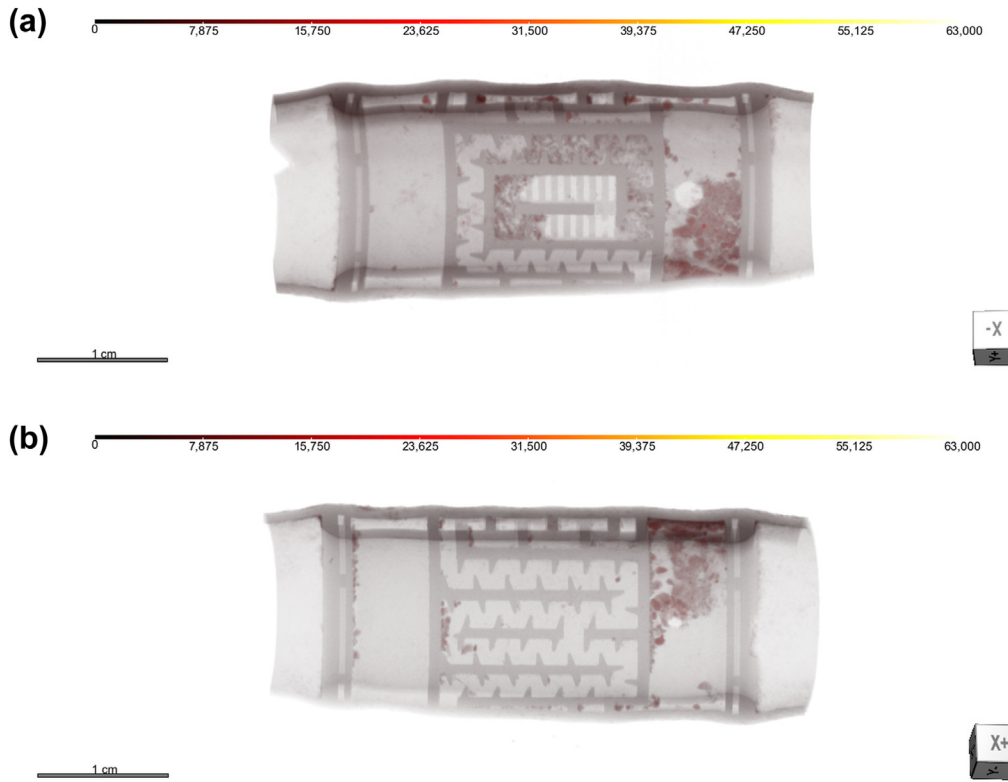
Figure 4. Surface geometry and clogging pattern of sample emitter 1, (a) side 1 and (b) side 2.

possible major source of Ca is chemical deposition of $CaCO_3$, whereas the other four elements originated primarily from suspended particles in water.

Among the four emitter samples, sample 2 exhibited quite a different proportion of Si and Ca elements. Figure 8 presents a plot with the mass percentage of Si, Al, K, Fe and Ca for each emitter sample. Emitters 1,3 and 4 have similar proportions of these five elements. But, sample 2 recorded very low proportion of Si, Al, K and Fe and high proportion of Ca. pH and CH values of source water seem to have less influence, but the geometry of the emitter. It is also noticed that, despite the difference in
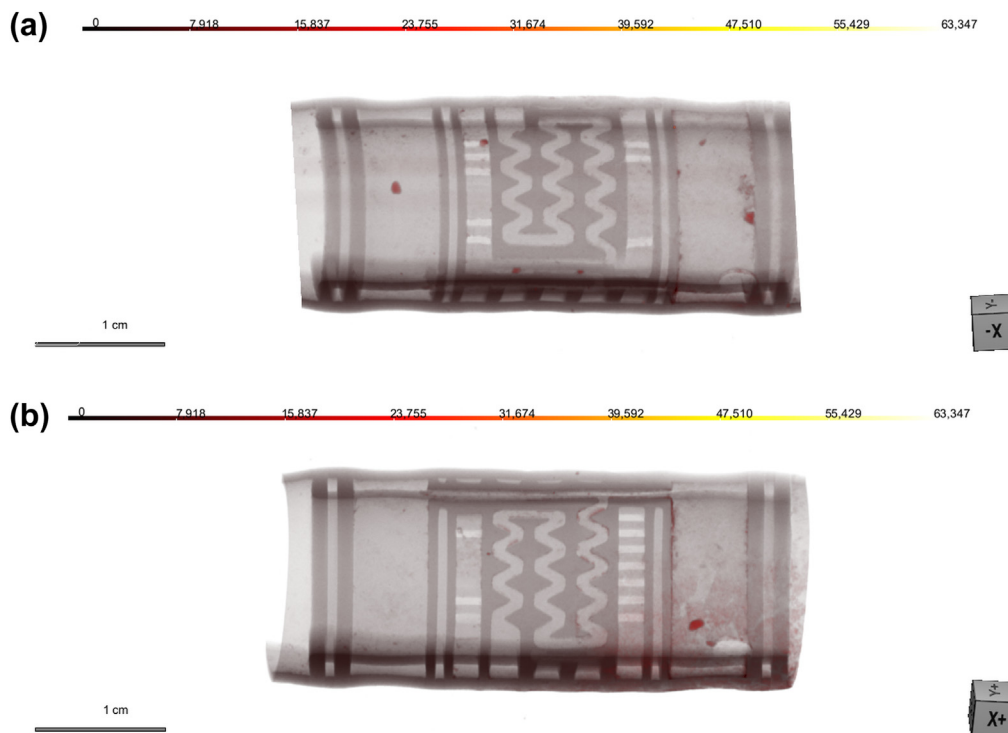
Figure 5. Surface geometry and clogging pattern of sample emitter 2, (a) side 1 and (b) side 2.

(a)

(b)
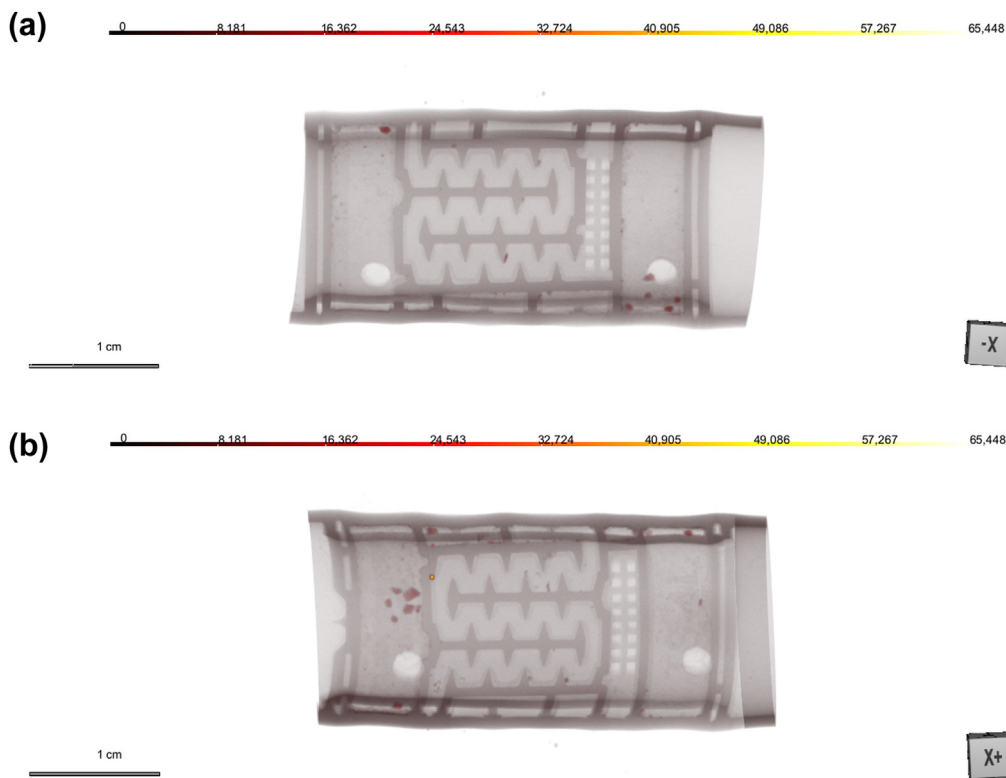
Figure 6. Surface geometry and clogging pattern of sample emitter 3, (a) side 1 and (b) side 2.

years of use of emitters 1,3 and 4, the proportion of five elements remained more or less unchanged. The probability of physical clogging material inhibiting the precipitation of $CaCO_3$ cannot be ruled out.

The inverse proportionality observed among physical and chemical clogging elements needs to be seen in relation with the emitter geometries. As analyzed before, the emitters 1,3 and 4 have similar labyrinth flow paths, whereas emitter 2 has narrower flow paths with curved boundaries. Thus, there is indication that such a flow path may help in flushing out most of the suspended matter in the water to the outlet and excreted as well through the emitter outlet. Also, it

(a)

(b)

Figure 7. Surface geometry and clogging pattern of sample emitter 4, (a) side 1 and (b) side 2.

Table 3. Comparison of geometric and clogging properties of four sample emitters.

Property	Sample 1	Sample 2	Sample 3	Sample 4
Location of inlet(s)	Center of the emitter	On either side of flow paths	On one side of the flow paths	On one side of the flow paths
Number of inlet(s)	One	Two	Four	Four
Number of outlet(s)	Two	Two	Four	Four
Direction of labyrinth flow paths	Both longitudinal and transverse	Transverse	Longitudinal	Longitudinal
Width of flow path (b) in Mm	1.183	0.893	1.472	1.472
Shape of the flow path	Zig-zag with sharp dentate tips and straight boundaries	Smooth curve shaped boundaries with less-sharper dentate tips	Zig-zag with sharp dentate tips and straight boundaries	Zig-zag with sharp dentate tips and straight boundaries
Dentate shape	Triangular with a right-angle at the base	Triangular	Triangular	Triangular
Dentate height (h) in Mm	1.129	1.263	1.431	1.431
Dentate angle (Θ)	36.792º	64.944º	38.495º	38.495º
Dentate spacing (s) in Mm	2.366	3.261	2.855	2.855
Area of deposition of clogging material	At inlet, labyrinth path near inlet and outlet areas	On outlet area and exit of flow path into outlet area	On two outlet areas on either side of the emitter. More of low-density clogging material	On two outlet areas on either side of the emitter. Deposition on inner surface of the emitter

Table 4. EDXRF analysis of elemental composition (mass percentage) in powder samples.

Sl.	Element	Sample 1	Sample 2	Sample 3	Sample 4	Sample 5
1	Silicon (Si)	61.843	23.235	60.822	57.454	0.958
2	Aluminum (Al)	12.636	5.312	11.683	11.549	0.000
3	Potassium (K)	11.767	2.534	9.824	8.963	0.000
4	Iron (Fe)	7.711	6.398	8.516	10.113	0.171
5	Calcium (Ca)	3.104	60.288	6.317	8.838	96.795
6	Titanium (Ti)	1.328	0.830	1.065	1.340	0.000
7	Sulfur (S)	0.959	0.403	0.840	0.966	0.264
8	Zirconium (Zr)	0.203	0.071	0.285	0.120	0.000
9	Manganese (Mn)	0.131	0.212	0.110	0.151	0.000
10	Vanadium (V)	0.062	0.068	0.059	0.084	0.000
11	Rubidium (Rb)	0.062	0.000	0.047	0.030	0.000
12	Strontium (Sr)	0.059	0.506	0.111	0.088	1.673
13	Thorium (Th)	0.046	0.000	0.000	0.000	0.000
14	Copper (Cu)	0.043	0.060	0.031	0.047	0.064
15	Zinc (Zn)	0.039	0.084	0.037	0.077	0.076
16	Yttrium (Y)	0.006	0.000	0.011	0.000	0.000
17	Erbium (Er)	0.000	0.000	0.242	0.178	0.000

may be inferred that while the physical particles were flushed out efficiently by the emitter, temperature-induced $CaCO_3$ deposition accumulated over time, predominantly during no-irrigation periods, resulting in much higher Ca proportion in the emitter clogging material.

3.4. Phase analysis using XRD

Figure 9(a), (b), (c), (d) present the XRD spectra of clogging material from the four emitter samples and Figure 9(e) presents the XRD spectrum of the powder sample 5 which is a mixture of extracts from the exteriors of all the four emitter assemblies. Samples 1,3 and 4 exhibited quite

Table 5. Correlation coefficients and p-values of five major elements.

Element	Si	Al	K	Fe	Ca
Si	1.0000				
Al	0.9968[a] (0.00021)[b]	1.0000			
K	0.9824 (0.00280)	0.9776 (0.00402)	1.0000		
Fe	0.9035 (0.03547)	0.9196 (0.02706)	0.8178 (0.09076)	1.0000	
Ca	-0.9995 (0.00001)	-0.9986 (0.00006)	-0.9795 (0.00350)	-0.9139 (0.02994)	1.0000

Note 1: Si = Silicon; Al = Aluminum; K = Potassium; Fe = Iron; and Ca = Calcium.
Note 2: The values in the upper triangle of the above table are left blank as they are identical to the corresponding values in the lower triangle.
  [a] linear correlation coefficient.
  [b] p-value corresponding to the correlation coefficient.
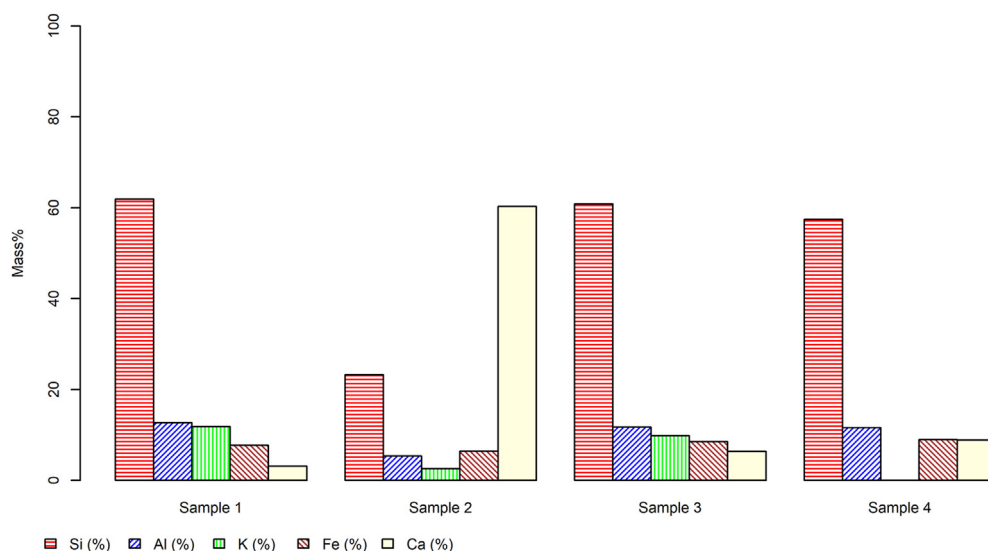
Figure 8. Proportion of chemical elements in clogging material.
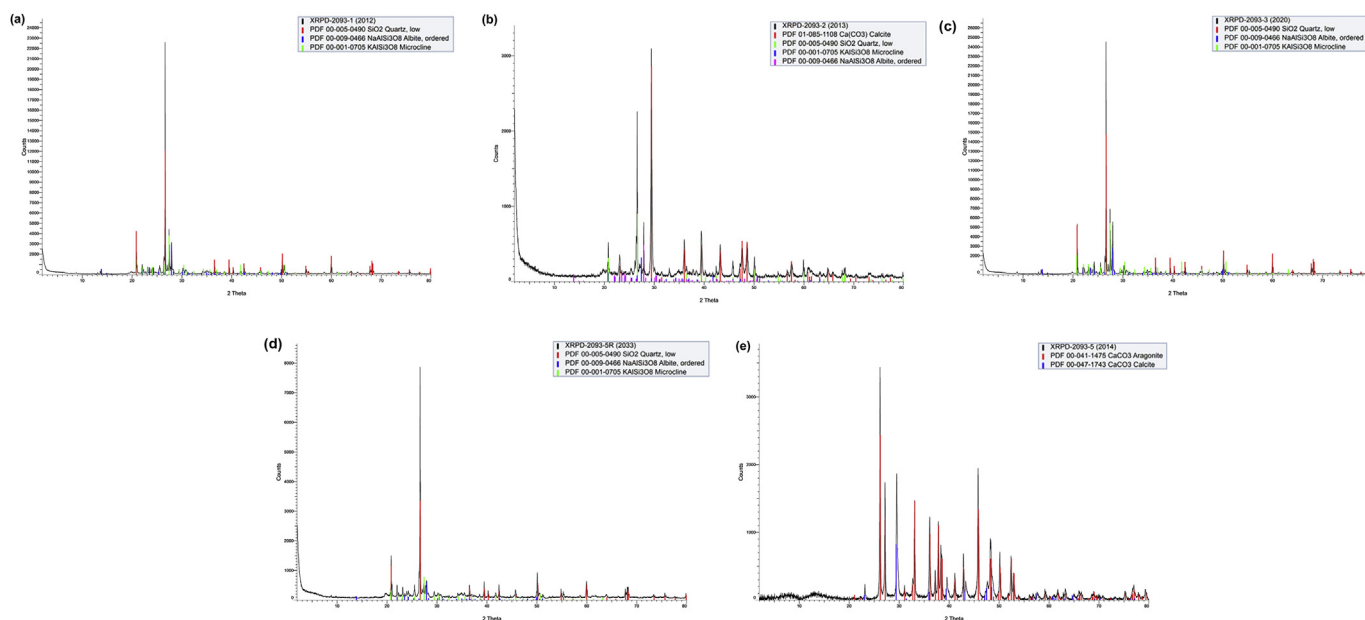
Figure 9. XRD spectrum of clogging material from emitters (a) sample 1, (b) sample 2, (c) sample 3, (d) sample 4, and (e) sample 5.

similar spectral properties and found to contain Quartz (SiO$_2$), Albite (NaAlSi$_3$O$_8$) and Microcline (KAlSi$_3$O$_8$) as dominant crystalline phases. The major chemical elements (Si, Al, K) found through an EDXRF analysis match with the elements in the crystal compounds found through XRD analysis. While Na, as in Albite, was not found through EDXRF due to detector limitations. Fe and Ca present in EDXRF results in small quantities ($\leq$10%), did not appear as constituents in XRD spectra. This indicates that there is a presence of amorphous compounds containing elements Fe and Ca.

The XRD spectrum of sample 2 stands out from that of sample 1,3 and 4. Visual observations reveal that several spectral peaks match with those of sample 1,3 and 4. Presence of Ca peaks in high counts was also found. Apart from Quartz (SiO$_2$), Albite (NaAlSi$_3$O$_8$) and Microcline (KAlSi$_3$O$_8$), the Calcite phase of CaCO$_3$ is one of the dominant constituents. EDXRF results also confirm that Ca is relatively larger in composition than Si, Al and K.

Lastly, qualitative phase analysis of XRD spectrum of sample 5 indicated presence of a combination of only two of the crystal phases of

CaCO$_3$, Calcite and Aragonite. EDXRF results, with 96.8% of the sample as Ca compound, confirm this result. This power sample is from the exteriors around the outlets of emitter assemblies. Evaporation of residual water drops due to sunlight and wind had caused the formation of this predominantly crystalline powder. But, the insides of emitters are not directly exposed to sunlight and wind. Hence, the physio-chemical process behind CaCO$_3$ precipitation needs to be studied more in detail. The possibility of natural bio-mineralization of CaCO$_3$, as narrated by Dhami et al. (2013), in the emitter flow paths during no-irrigation periods cannot be ruled out.

From XRD analysis of powder samples of unknown composition, one cannot easily decipher the amorphous constituents. In all, while it is not possible to guess how much of Ca present in the samples 2 and 5 is amorphous, it is no guess that Ca is present in samples 1,3 and 4. It is known that Calcium Carbonates exist either in the form of Amorphous Calcium Carbonate (ACC) or one of the three polymorphs, namely, Calcite, Aragonite, and Vaterite. Two hydrated phases of Calcium Carbonate Monohydrate (CaCO$_3$·H$_2$O), and Hexahydrate of Calcium

Carbonates ($CaCO_3\cdot 6H_2O$) are also possible forms of hydrated calcium carbonates. Detection of a new hydrated crystalline phase, hemihydrate $CaCO_3\cdot\frac{1}{2}H_2O$ was recently reported by Zou et al. (2019). Among the anhydrous polymorphs of $CaCO_3$, Calcite is thermodynamically the most stable followed by Aragonite and Vaterite at ambient conditions (Chang et al., 2017). ACC, Aragonite and Vaterite tend to transform to most stable Calcite phase, under favorable temperature, pH and ambient chemical conditions (Chang et al., 2017). Heating at high temperature was successfully used to transform the ACC to one or more of its polymorphs (Noel et al., 2013). Quantitative Rietveld analysis using internal standards or external standards, as detailed by Suherman et al. (2002) forms the future scope for bringing out the quantities of different phases of $CaCO_3$ deposited on the emitter surface.

4. Discussion

Examination of emitters used for several years in agricultural farms has the advantage of obtaining results that are representative of real field conditions. In the current study, four cylindrical emitters by two major companies in India were randomly studied, without the knowledge of variations in emitter geometries before carrying out the CT scanning.

pH and CH are known as causative factors in chemical clogging of emitters. But, the pH of water samples and the proportion of Ca in clogging material does not seem to correlate. The CH values of four source water samples are in the range of 280–430 mg L^{-1}, but do not exhibit any trend with the proportion of Ca in the corresponding clogging material. Emitters 1,3 and 4, which have a similar labyrinth path width and geometric features have Ca in the range of 3.1–8.8%. But, emitter 2 with low physical clogging material on it, has very high proportion of Ca. Thus, emitter geometry seems to exhibit better correlation with the proportion of Ca in the clogging material. The presence of a more proportion of Ca found in such emitters indicates accumulation of chemical clogging over time. This chemical precipitation on emitter flow paths and outlet areas could happen during no-irrigation phase, as a result of exposure to heat and/or bio-mineralization.

Despite its limitations, the current study is unique as it exposed the proportional relation between physical and chemical clogging of emitters. The EDXRF revealed relative quantities of chemical elements, but not the composition of chemical compounds. XRD analysis supplements EDXRF in identifying the chemical composition of compounds, particularly those in crystalline form. EDXRF and XRD together facilitate to infer that the three major elements, Si, Al and K, have their source in physical clogging caused by suspended particles in water. On the contrary, Ca could be predominantly originated from the CC whose source is in the water. The XRD analysis confirmed that most of the Ca present in the emitter clogging material is in the form of crystalline $CaCO_3$, though minor presence of ACC in the clogging material could be a possibility. The element Fe is also present in EDXRF but not in any of the crystalline compounds in XRD analysis. It may be inferred that compounds of Fe are present in amorphous form. Quantitative analysis of XRD data helps us to further explore this aspect.

The CT scans revealed that the deposition of clogging material is more towards and on the outlets. Thus, it is important to consider the outlet areas also while designing cylindrical emitters for anti-clogging properties. Excretion of physical clogging materials seems to be more efficient with the emitter having boundary optimized using small curvature; narrower flow paths; larger dentate angle and wider dentate spacing. This finding agrees fairly with the CFD-based results of Feng et al. (2018) which concluded that narrower flow paths with higher average flow velocities and curved boundaries facilitate efficient removal of physical clogging material. This finding is also consistent with of Yang et al. (2020). However, it is important to note that both Feng et al. (2018) and Yang et al. (2020) did not consider the outlet areas in their CFD models in assessing the anti-physical-clogging performance of emitters. The influence of the direction of flow (with respect to the flow in lateral tube) on the clogging behavior of emitters needs further study.

The combined application of CT, EDXRF and XRD techniques for understanding the emitter geometry, composition and crystalline phases is found to be promising, but not devoid of some challenges. Since the clogging material had to be extracted by physically cutting and destroying the sample emitter assemblies, this cannot be treated as an entirely non-destructive method. Theoretically, the powder extracts obtained from the emitters are a mix of different compounds, whose source could be either SS in the water or due to precipitation of dissolved salts in the water. Based on the EDXRF and XRD analysis, it is not possible to precisely identify the source of clogging material. But they gave reasonable insight into the relative proportion of physical and chemical clogging and probable source of the chemical elements found. For example, it may be inferred logically that the major source of Ca is from the precipitation of $CaCO_3$ in water, while Si is from the silt particles that passed through the filters and carried by water in suspended form.

By taking a randomized sampling approach, though inconclusive in certain aspects, current study successfully demonstrates the potential of non-destructive testing methods in studying the drip emitter clogging problem. This study contributes to better understanding of the processes in clogging and possible relation between different forms of clogging. A larger and structured study may be taken up to further verify whether the physical clogging and chemical clogging relationship holds good at different SS, TH, CH and pH levels of source water and for different emitter geometries.

5. Conclusion

i. The potential of combined application of CT, EDXRF and XRD techniques for understanding the emitter geometry, clogging material deposition pattern on the emitter surface and its composition is found to be promising.

ii. Excretion of physical clogging materials seems to be more efficient with the emitter having boundary optimized using small curvature; narrower flow paths and larger dentate angle as well as spacing. However, the presence of a more proportion of $CaCO_3$ found in such emitters indicates accumulation of chemical clogging over time.

iii. The composition analysis of clogging material found to be useful to study the relative proportion of physical and chemical clogging materials and their possible relation to emitter geometry. The inverse proportionality between quantities of physical clogging and chemical clogging materials highlights the need for directing the efforts of modelling and designing emitters not only against physical clogging, but also chemical clogging.

iv. The CT scans revealed that the deposition of clogging material is more towards and on the outlets. Thus, it is important to consider the outlet areas also while modelling and designing emitters for anti-clogging properties.

Data availability statement

All the data, models or code that supports the findings of this study are available from the corresponding author upon reasonable request. These are - (i) the raw scan data of emitter samples and extracts on CT, XRD and EDXRF equipment and (ii) the R code written for generating the graphics.

Declarations

Author contribution statement

Venkata Ramamohan Ramachandrula: Conceived and designed the experiments; Performed the experiments; Analyzed and interpreted the data; Contributed reagents, materials, analysis tools or data; Wrote the paper.

Ramamohan Reddy Kasa: Conceived and designed the experiments; Analyzed and interpreted the data.

Competing interest statement

The authors declare no conflict of interest.

Additional information

No additional information is available for this paper.

References

APHA, 2012. Standard Methods for the Examination of Water and Waste Water. American Public Health Association, Washington, DC.

Bounoua, S., Tomas, S., Labille, J., Molle, B., Granier, J., Haldenwang, P., Izzati, S.N., 2016. Understanding physical clogging in drip irrigation: in-situ, in-lab and numerical approaches. Irrigat. Sci. 34 (4), 327–342.

Bucks, D.A., Nakayama, F.S., Gilbert, R.G., 1979. Trickle irrigation water quality and preventive maintenance. Agric. Water Manag. 2, 149–162.

Bui, W., 1988. Results of drip irrigation tubing evaluation program in the Hawaiian sugar industry. In: Proc., 4th International Micro Irrigation Congress. 4 (A-3). International Commission on Irrigation and Drainage, Albury-Wodonga, Australia.

Bunaciu, A.A., Udriştioiu, E.G., Aboul-Enein, H.Y., 2015. X-ray diffraction: instrumentation and applications. Crit. Rev. Anal. Chem. 45 (4), 289–299.

Chang, R., Kim, S., Lee, S., Choi, S., Kim, M., Park, Y., 2017. Calcium carbonate precipitation for CO_2 storage and utilization: a review of the carbonate crystallization and polymorphism. Front. Energy Res. 5, 17.

Dazhuang, Y., Peiling, Y., Shumei, R., Yunkai, L., Tingwu, X., 2007. Numerical study on flow property in dentate path of drip emitters. NZJAR (N. Z. J. Agric. Res.) 50 (5), 705–712.

de Camargo, A.P., Molle, B., Tomas, S., Frizzone, J.A., 2014. Assessment of clogging effects on lateral hydraulics: proposing a monitoring and detection protocol. Irrigat. Sci. 32 (3), 181–191.

Dhami, N.K., Reddy, M.S., Mukherjee, M.S., 2013. Biomineralization of calcium carbonates and their engineered applications: a review. Front. Microbiol. 4, 1–13.

Feng, J., Sun, H., Li, Y., 2013. Visualizing particles movement characteristics in drip irrigation emitters with digital particle image velocimetry [in Chinese] Trans. Chin. Soc. Agric. Eng. 29 (13), 90–96.

Feng, J., Li, Y., Liu, Z., Muhammad, T., Wu, R., 2019. Composite clogging characteristics of emitters in drip irrigation systems. Irrigat. Sci. 37, 105–122.

Feng, J., Li, Y., Wang, W., Xue, S., 2018. Effect of optimization forms of flow path on emitter hydraulic and anti-clogging performance in drip irrigation system. Irrigat. Sci. 36 (1), 37–47.

Kirnak, H., Doğan, E., Demir, S., Yalçin, S., 2004. Determination of hydraulic performance of trickle irrigation emitters used in irrigation systems in the Harran plain. Turk. J. Agric. For. 28 (4), 223–230.

Krishna Reddy, Y.V., Adamala, S., Babu, B.H., 2017. Case study on performance evaluation of drip irrigation systems in selected villages of Guntur district, Andhra Pradesh, India. Int. J. Curr. Microbiol. App. Sci. 6 (2), 437–445.

Li, G., Wang, J., Alam, M., Zhao, Y., 2006. Influence of geometrical parameters of labyrinth flow path of drip emitters on hydraulic and anti-clogging performance. Trans. ASABE. 49 (3), 637–643.

Liu, H., Huang, G., 2019. Laboratory experiment on drip emitter clogging with fresh water and treated sewage effluent. Agri. Water Mgt. 96 (5), 745–756.

Liu, Y., Li, D., Wu, P., Zhang, L., Zhu, D., Chen, J., 2018. Clogging characteristics of different emitters in drip irrigation with hard water [in Chinese] Trans. Chin. Soc. Agric. Eng. 34 (3), 96–102.

Liu, Y., Wu, P., Zhu, D., Zhang, L., Chen, J., 2015. Effect of water hardness on emitter clogging of drip irrigation [in Chinese] Trans. Chin. Soc. Agric. Eng. 31 (20), 95–99.

Li, Y., Feng, J., Xue, S., Muhammad, T., Chen, X., Wu, N., Li, W., Zhou, B., 2019a. Formation mechanism for emitter composite-clogging in drip irrigation system. Irrigat. Sci. 37, 169–181.

Li, Y., Pan, J., Chen, X., Xue, S., Feng, J., Muhammad, T., Zhou, B., 2019b. Dynamic effects of chemical precipitates on drip irrigation system clogging using water with high sediment and salt loads. Agri. Water Mgt. 213 (1), 833–842.

Li, Y., Xu, H., Lin, X., Xu, T., Wei, R., Yang, P., Ren, S., 2008. CFD and digital particle tracking to assess flow characteristics in the labyrinth flow path of a drip irrigation emitter. Irrigat. Sci. 26 (5), 427–438.

Nakayama, F.S., Bucks, D.A., 1991. Water quality in drip/trickle irrigation: a review. Irrigat. Sci. 12, 187–192.

Nguyen, T.T., Indraratna, B., 2019. Micro-CT scanning to examine soil clogging behavior of natural fiber drains. J. Geotech. Geoenviron. Eng. 145 (9), 04019037.

Noel, E.H., Kim, Y.Y., Charnock, J.M., Meldrum, F.C., 2013. Solid state crystallization of amorphous calcium carbonate nanoparticles leads to polymorph selectivity. CrystEngComm 15 (4), 697–705.

Patil, S.S., Nimbalkar, P.T., Joshi, A., 2013. Hydraulic study, design & analysis of different geometries of drip emitter labyrinth. Int. J. Eng. Adv. Technol. 2 (5), 455–462.

Ramachandrula, V.R., Kasa, R.R., 2019a. Parameters influencing chemical clogging of drip emitters: an exploratory field study. In: Proc., 9th International Micro Irrigation Conf. (9IMIC) (Ed.), Indian National Committee on Surface Water (INCSW) and Central Water Commission (CWC). IvyLeagueSystems, Aurangabad, India, pp. 431–436.

Ramachandrula, V.R., Kasa, R.R., 2019b. Application of Computed Tomography to study drip emitter geometry and clogging. In: Gopal Naik, M., Suresh Kumar, N., Anjaneya Prasad, M., Raja Sekhar, P., Shashikanth, P., Prasanna, S.V.S.N.D.L., Guptha, H. (Eds.), Proc., 5th HYDRO Conf. Dept. of Civil Engg., OU and Indian Society for Hydraulics, Hyderabad, India, pp. 978–986.

Reethi, K., Mallikarjuna, Vijaya Raghu, S., 2015. Analysis of flow through a drip irrigation emitter. Int. J. Mod. Eng. Res. 5 (11), 57–64.

Shaw, A., Ghosh, U., Biswas, R.K., 2018. Study on clogging problem of drip irrigation systems and its remedies. Int. J. Curr. Microbiol. App. Sci. 7 (8), 1934–1941.

Suherman, P.M., van Riessen, A., O'Connor, B., Li, D., Bolton, D., Fairhurst, H., 2002. Determination of amorphous phase levels in Portland cement clinker. Powder Diffr. 17 (3), 178–185.

Wei, Q., Shi, Y., Lu, G., Dong, W., Huang, S., 2008. Rapid evaluations of anticlogging performance of drip emitters by laboratorial short-cycle tests. J. Irrigat. Drain. Eng. 134 (3), 298–304.

Xiao, Y., Sawicka, B., Liu, Y., Zhou, B., Hou, P., Li, Y., 2020. Visualizing the macro-scale spatial distributions of biofilms in complex flow channels using industrial computed tomography. Biofouling 36 (2), 115–125.

Yang, B., Wang, J., Zhang, Y., Wang, H., Ma, X., Mo, Y., 2020. Anti-clogging performance optimization for dentiform labyrinth emitters. Irrigat. Sci. 38, 275–285.

Yavuz, M.Y., Demirel, K., Erken, O., Bahar, E., Deveciler, M., 2010. Emitter clogging and effects on drip irrigation systems performances. Afr. J.Agri. Res. 5 (7), 532–538.

Yu, L., Li, N., Long, J., Liu, X., Yang, Q., 2018. The mechanism of emitter clogging analyzed by CFD–DEM simulation and PTV experiment. Adv. Mech. Eng. 10 (1), 1–10.

Zhangzhong, L., Yang, P., Zhen, W., Zhang, X., Wang, C., 2019. A kinetic model for the chemical clogging of drip irrigation system using saline water. Agri. Water Mgt. 223 (20), 105696.

Zhou, B., Wang, D., Wang, T., Li, Y., 2018. Chemical clogging behavior in drip irrigation systems using reclaimed water. Trans. ASABE. 61 (5), 1667–1675.

Zou, Z., Habraken, W.J.E.M., Matveeva, G., Jensen, A.C.S., Bertinetti, L., Hood, M.A., Sun, C.Y., Gilbert, P.U.P.A., Polishchuk, I., Pokroy, B., Mahamid, J., Politi, Y., Weiner, S., Werner, P., Bette, S., Dinnebier, R., Kolb, U., Zolotoyabko, E., Fratzl, P., 2019. A hydrated crystalline calcium carbonate phase: calcium carbonate hemihydrate. Science 363, 396–400.